Atmospheric Research 259 (2021) 105676

Contents lists available at ScienceDirect

Atmospheric Research

journal homepage: www.elsevier.com/locate/atmosres

Estimating near-surface climatology of multi-reanalyses over the Greenland Ice Sheet

Wuying Zhang [a], Yetang Wang [a,*], Paul C.J.P. Smeets [b], Carleen H. Reijmer [b], Baojuan Huai [a], Junyao Wang [a], Weijun Sun [a,*]

[a] College of Geography and Environment, Shandong Normal University, Jinan 250014, China
[b] Institute for Marine and Atmospheric Research, Utrecht University, Utrecht, the Netherlands

ARTICLE INFO

Keywords:
Air temperature
Relative humidity
Wind speed
Reanalysis products
Greenland Ice Sheet

ABSTRACT

This study uses meteorological records from Automatic Weather Stations (AWSs) to estimate the performance of global reanalysis products for monthly air temperature, relative humidity and wind speed over the Greenland Ice Sheet (GrIS). These products include the fifth generation European Centre for Medium-Range Weather Forecasts (ECMWF) reanalysis (ERA5), ECMWF Interim Reanalysis (ERAI), Modern-Era Retrospective Analysis for Research and Applications, Version 2 (MERRA-2), Climate Forecast System Reanalysis Version 1/Climate Forecast System Version 2 (CFSRv1/CFSRv2), and Japanese 55-year Reanalysis (JRA-55). The global reanalysis products generally perform better in summer than in winter, and their qualities vary by glaciological regime. No reanalysis is clearly identified as the optimal dataset for all meteorological parameters, seasons and regions. For all reanalyses, warm biases are observed in the accumulation zone, but cold biases are observed in the ablation area of the GrIS. ERAI, ERA5 and JRA-55 underestimate relative humidity during any month. While MERRA-2 overestimates wind speeds, underestimates are found for the other reanalyses excluding JRA-55 during all months. Despite the robust agreement between the AWS time series for all three variables and each reanalysis product averaged over the ice sheet, sudden jumps occur in annual mean wind speed in CFSR, and in annual relative humidity in JRA-55 from 2010 to 2011.

1. Introduction

The Greenland Ice Sheet (GrIS), the largest ice body in the Northern Hemisphere, is losing mass at an accelerated rate and contributed to 20–25% of the rise in the global sea level, during the past few decades. This contribution is expected to increase over the coming decades and centuries (IPCC, 2019). The key mechanism is ice flow acceleration induced by surface melting and ocean ice flow by bottom calving, which is driven by the warming Arctic atmospheric conditions (Gillet-Chaulet et al., 2012; Ren et al., 2011). Under the background of sustained climate warming, the ice sheet is becoming increasingly vulnerable to the frequent occurrence of weather extremes (Overland and Wang, 2016; Hanna et al., 2018). This has raised widespread concern regarding the investigation of changes in the weather and climate and of anomalous weather patterns over the GrIS. However, sparseness of in situ observation data is a primary challenge to understanding the state, anomalies, and variations of weather and climate over the ice sheet, because of the logistical difficulties in the remote and extreme environments. As a result, long-term climate observations are only available at ten weather stations distributed over the coastal zones, which cannot provide direct information on the conditions of the vast interior. To address this, continuous weather measurements have been made over the inland GrIS from 1995 onwards, but many glaciological regimes are still undocumented.

To fill in gaps of sparse observations of the GrIS, atmospheric reanalysis products are an important alternative to represent the spatially and temporally complete state of the atmosphere. They have been widely used to force regional climate models to gain better insight into the mechanism of variability in the GrIS surface mass balance and climate in recent decades. At present, there are a number of high-resolution reanalysis datasets available to the public, such as the Japan Meteorological Agency 55-year Reanalysis (JRA-55) (Kobayashi et al., 2015), the Climate Forecast System Reanalysis (CFSR) (Saha et al., 2010), National Aeronautics and Space Administration the Modern-Era

* Corresponding authors.
E-mail addresses: yetangwang@sdnu.edu.cn (Y. Wang), sun1982wj@163.com (W. Sun).

https://doi.org/10.1016/j.atmosres.2021.105676
Received 8 February 2021; Received in revised form 3 May 2021; Accepted 7 May 2021
Available online 12 May 2021

Retrospective Analysis for Research and Applications 2 (MERRA-2) (Gelaro et al., 2017), the European Centre for Medium-Range Weather Forecast (ECMWF) 'Interim' reanalysis (ERAI) (Dee et al., 2011), and the fifth generation ECMWF reanalysis models (ERA5) (Hersbach and Dee, 2016). Despite the application of the assimilation schemes and a numerical weather prediction models, the reanalysis datasets are known to have uncertainties, especially at high latitudes with limited observation constraints. Uncertainties in the reanalysis datasets also greatly affect the performance of the regional climate models because these models are sensitive to the forcing fields used. Thus, validation of the reanalysis products is required before they are used to investigate climate changes, and to force climate models.

Some previous studies have focused on the assessment of the performance of reanalysis datasets for the GrIS. For example, Delhasse et al. (2019) compared the relative skill of ERA-Interim and ERA5 for capturing GrIS air temperature and wind speeds from 2010 to 2016. Eyre and Zeng (2017) evaluated the performance of seven global reanalyses (not including ERA5) and other model datasets for near-surface air temperature base on in-situ observations. Hearty et al. (2018) provided an evaluation of the representation of AIRS, MERRA, and MERRA-2 three reanalysis products for 2 m air temperature at summit. However, considerable gaps in knowledge still exist regarding the relative performance of recent reanalysis products for more meteorological variables over the GrIS.

The purpose of this study is to determine how well the performances of recent reanalysis products including JRA-55, CFSR, MERRA-2, ERAI and ERA5 for the climate over the GrIS agree with each other, based on in situ observations from AWSs, given that ice sheet mass balance processes are strongly influenced by air temperature (Van de Wal and Oerlemans, 1997; Chylek et al., 2004; Hanna et al., 2010), temperature, humidity and wind, which are associated with turbulent heat fluxes and turbulence (Johnson, 1995; Katul and Parlange, 1994; Takahashi et al., 2002). The relative humidity and wind speed play a key role in the variations of the heat budget components. For example, wind speed changes have an impact on the spatial variability in temperature, and then result in changes in the latent heat flux (Li et al., 2011). The wind activities usually alter the paths of water vapor transport into the GrIS. Furthermore, the water vapor flux income can be quantified based on wind speed, relative humidity and other factors. Therefore, we chose these three near-surface meteorological variables in the five reanalysis datasets for the estimation.

2. Data and methods

2.1. AWS data

We use meteorological records at 36 weather stations from three AWS networks, i.e., the Greenland Climate Network (GC–Net) (Steffen and Box, 2001), The Program for Monitoring the Greenland Ice Sheet (PROMICE) (Van As et al., 2011) launched by Geological Survey of Denmark and Greenland (GEUS) in 2007, and the K–transect in western Greenland by Utrecht University Institute for Marine and Atmospheric Research (Van de Wal et al., 2005; van den Broeke et al., 2011; Munneke et al., 2018). The spatial distribution of the 36 AWSs is shown in Fig. 1, and Table 1 summarizes the location, elevation and availability of data from these stations. AWSs provide the measurements of meteorological conditions at the approximately 2-3 m above the surface. The daily air temperature, relative humidity and wind speed data are obtained from the three AWS networks. To evaluate the GrIS climate changes in the reanalyses, the long-term and continuous records are essential. Here we select the AWS records spanning at least 10 years, although not necessarily continuous. All data are quality-controlled by the data providers. The main quality control for air temperature is to correct the biases caused by the overheating under the low wind speed and high solar insolation. As for relative humidity, a low-temperature bias correction is made based on air temperature and the saturation vapor pressure curves

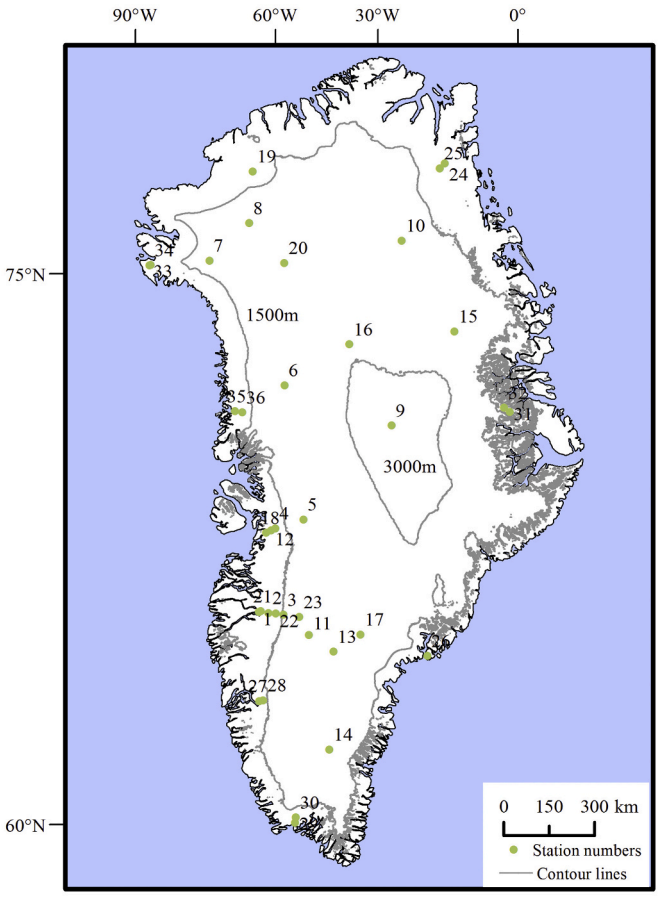

Fig. 1. Spatial distribution of AWS on the GrIS.

for the plane surface among the pure water-ice surface. For near surface temperature and relative humidity, correction algorithms, such as the model of Jacobs and McNaughton, are adapted to the underlying surface of ice. In addition, a rescaling method is used to eliminate the underestimation over the subfreezing environment. Corrections are also made for wind speed errors by anemometers overspeeding in turbulent flow, anemometers freezing and having screens covered by frost, and physical anomalies, etc. Detailed correction procedures can be found in Van de Wal et al. (2011). (See Table 2).

2.2. Reanalysis data

JRA-55 (Ebita et al., 2011; Kobayashi et al., 2015) is the second Japanese global atmospheric reanalysis conducted by the Japan Meteorological Agency (JMA) in December 2009. It is the successor of the Japanese 25-year Reanalysis (JRA-25), with the improvement of some deficiencies in JRA-25 such as large temperature biases in the lower stratosphere, and dry land surface anomalies in the Amazon basin. A four-dimensional variational (4D-Var) data assimilation scheme with T106 inner model is used to primarily assimilate the data that are used in ERA-40, and more recent observations. This dataset covers 1958 to present, and has the resolutions of TL319L60 (~60 km) in the horizon and 60 hybrid levels in verticality.

ERAI (Berrisford et al., 2011; Dee et al., 2011) is a reanalysis of the global atmosphere launched by the ECMWF in September 2006, with the aim of connecting ERA-40 with the next generation reanalysis. The assimilation scheme is Cy31R2 in the Integrated Forecast System (IFS) generated by ECMWF, which includes a 4D-Var data assimilation with 12 h analysis window. ERAI provides atmospheric estimations for the 1979–2019 period, with a horizontal resolution of T255 (~79 km) and

Table 1
Main characteristics of the AWS measurements.

Number	Station name	Latitude (N°)	Longitude (W°)	Elevation(m)	Time coverage
1	grl_aws05	67.08	50.10	527	Aug.2003- present
2	grl_aws06	67.07	49.38	1059	Aug.1997- present
3	grl_aws09	67.05	48.22	1538	Aug.2003- present
4	Swiss Camp	69.57	49.32	1158	Jan.1996- Jan.2018
5	Crawford Pt.	69.88	46.99	1997	Jan.1996- Jan.2018
6	NASA-U	73.84	49.50	2365	Jan.1996- Jan.2018
7	GITS	77.14	61.04	1932	Jan.1996- Jan.2018
8	Humboldt	78.53	56.83	1988	Jan.1996- Jan.2018
9	Summit	72.58	38.50	3249	May.1996- Jan.2018
10	TUNU-N	78.02	33.99	2112	May.1996- Jan.2018
11	DYE-2	66.48	46.28	2162	Jul.1996.7- Jan.2018
12	JAR	69.50	49.68	961	Jun.1997- Dec.2017
13	Saddle	66.00	44.50	2515	Apr.1997- Jan.2018
14	South Dome	63.15	44.82	2957	Apr.1997- Jan.2018
15	NASA-E	75.00	30.00	2663	May.1997- Jan.2018
16	NGRIP	75.10	42.33	2957	Jan.2002- Nov.2010
17	NASA-SE	66.48	42.50	2429	Apr.1998- Jan.2018
18	JAR 2	69.42	50.06	537	Jun.1996- May.2007
19	Peteman ELA	80.08	58.07	1006	May.2003- Dec.2017
20	NEEM	77.50	50.87	2475	Mar.2006- Jan.2018
21	Kan-L	67.10	49.95	715	Sep.2008- present
22	Kan-M	67.07	48.83	1300	Sep.2008- present
23	Kan-U	67.00	47.03	1884	Apr.2009- present
24	Kpc-L	79.91	24.08	411	Jul.2008- present
25	Kpc-U	79.83	25.17	901	Jul.2008- present
26	Mit	65.69	37.83	499	May.2009- present
27	Nuk-L	64.48	49.54	615	Aug.2007- present
28	Nuk-U	64.51	49.27	1174	Aug.2007- present
29	QAS-L	61.03	46.85	325	Aug.2007- present
30	QAS-U	61.18	46.82	963	Aug.2008- present
31	Sco-L	72.22	26.82	1868	Jul.2008- present
32	Sco-U	72.39	27.23	1054	Jul.2008- present
33	Thu-L	76.40	68.27	585	Aug.2010- present
34	Thu-U	76.42	68.15	778	Aug.2010- present
35	Upe-L	72.89	54.30	235	Aug.2009- present
36	Upe-U	72.89	53.58	1017	Aug.2009- present

vertical 60 levels from the surface up to 0.1 hPa.

ERA5 (Hennermann and Berrisford, 2017) is the latest ECMWF reanalysis for the representation of global weather and climate and has replaced ERAI. It provides hourly data of a large amount of meteorological parameters on the atmosphere, land and ocean, together with uncertainty evaluation. The dataset is generated by a 4D-Var ensemble of data assimilation with ten members and the high-resolution forecasts in the IFS CY41r2, with a resolution with 137 hybrid sigma-pressure (model) levels in the vertical direction. Currently, ERA5 spans from 1950 onwards. Its resolution is TL639 (~31 km), and TL319 (~63 km) for the ensemble members in the horizontal direction, and 137 levels up to a top level of 0.01 hPa in the vertical direction, respectively.

CFSR (Saha et al., 2006; Saha et al., 2014) has two versions, CFSR version 1 (CFSRv1) and its successor version 2 (CFSv2). CFSRv1 and CFSRv2 cover the period between 1979 and 2010, and from 2011 to the present, respectively. CFSRv1 was implemented by the National Centers for Environmental Prediction (NCEP) in August 2004 and is regarded as the first-global, fully coupled atmosphere- ocean-land model used at NCEP for seasonal prediction. The CFSv2 is completed in March 2011. Relative to CFSRv1, many improvements have been made on almost all aspects of the data assimilation and forecast model system, especially for the consistency between model states and the original states. Both datasets have the resolutions of T382 (~38 km) in the horizontal and 64 vertical levels with the highest level at 0.266 hPa.

Spanning from 1980 onwards, MERRA-2 (Gelaro et al., 2017) is released by the NASA's Global Modeling and Assimilation Office (GMAO). The aim of MERRA-2 project is to provide a better dataset to replace the former version, MERRA. To achieve this goal, the MERRA-2 assimilates observation types which are not available for its predecessor, and updates the Goddard Earth Observing System (GEOS) analysis scheme and model. The spatial resolution of MERRA-2 is 0.5° × 0.67° (~55 km). Compared with MERRA, MERRA-2 makes several improvements including a reduction in biases and imbalances in the observation system and water cycle.

2.3. Methods

Due to the relatively coarse resolution, biases occur in the surface elevation fields of the reanalysis products, relative to the actual topography of Greenland. The elevation biases result in the difference between reanalyzed air temperature and the actual one. To account for this, corrections are made based on the environmental lapse rate of 6.5 °C/km.

Bilinear interpolation is used to extract the reanalysis data at the corresponding station locations. Near-surface relative humidity is unavailable in ERAI, ERA5 and MERRA-2, instead, 2 m dew temperature is available and near-face relative humidity is calculated by the following formula.

$$RH = 100*es(Td)/es(T) \quad (1)$$

where RH, es(Td), and es(T) are relative humidity, the saturation vapor pressure of dew point temperature, and air temperature, respectively. The formula for calculating the saturation vapor pressure of ice below 0 °C is as follows:

$$es = es_0*10[at/(b+t)] \quad (2)$$

where $a = 9.5$, $b = 265.5$, $es_0 = 6.11$(saturated water pressure under 273.15 K), and t is the temperature in centigrade (Marray, 1967).

AWS wind speed measurements are nominally measured at 3 m above the surface (Lazzara et al., 2012). Thus corrections are required

Table 2
Summary of characteristics of reanalysis products used in this study.

Name	Organization	Horizontal resolution	Vertical resolution	Assimilation system	Period
JRA-55	JMA	TL319; 55 km	60	4D-Var	1958–present
ERAI	ECMWF	T255; 79 km	60	4D-Var	1979–2019
ERA5	ECMWF	TL319; 31 km	137	4D-Var	1950–present
CFSR	NCEP	T382; 38 km	64	3D-Var	1979–present
MERRA-2	NASA/GMAO	0.5°*0.67°; 55 km	72	3D-Var	1980–present

before comparison with a height of 10 m wind speeds from the reanalysis datasets. We extrapolate the AWS wind speed observations to 10 m height based on a power law wind profile assuming neutral atmospheric conditions (Paulson, 1970; Sanz Rodrigo, 2011).

$$WS(h) = WS(h_{ref})\left[h/h_{ref}\right]^{\alpha} \quad (3)$$

where h_{ref} is the height of the reanalysis wind speed (10 m). h is the height of the AWS measurement. Alpha (α) is a non-dimensional wind-shear exponent. A value of α is 0.143 was used for land (Touma, 1977; Dong et al., 2020), and an a value of 0.11 is used for water (Hsu et al., 1994).

Indicators including the mean bias (MB) and root-mean-square error (RMSE) are used to quantify the performance of the reanalysis datasets, relative to in-situ measurements. The indicators are only calculated for their overlapping periods. When computing the indicators, the AWSs are divided into two groups based on elevation of the stations over 1500 m and below 1500 m. The 1500 m elevation is selected because it represents the average glacier equilibrium line altitude of the GrIS (Eyre and Zeng, 2017; Van de Wal et al., 2005). We calculate area weighted averages of annual near surface temperature, relative humidity and wind speed in all reanalysis datasets at the ice sheet scale to make a comparison of their temporal variability with each other.

3. Results

3.1. Performance of the reanalysis products with respect to observations

3.1.1. Air temperature

Fig. 2 shows the intra-annual cycle of MB and the RMSE of air temperature in the five reanalysis datasets. The MB and RMSE of all datasets exhibit seasonality-dependent patterns. For the accumulation area (Fig. 2a and c, Table 3a), all datasets have the smallest MB and RMSE values in summer, and the largest values occur in winter. MB values of both ERAI and MERRA-2 are positive for any month, i.e., warm biases occur in the two reanalyses. For the other three reanalysis products, cold biases are observed during summer, but warm biases are observed during winter. In the accumulation area, the seasonal cycle of RMSE for any reanalysis product is common, peaking in winter months with small values in summer months. The RMSEs of ERAI and ERA5 are similar, which suggests that there is no significant improvement in the performance of ERA5 for air temperature, compared with ERAI. By comparison, MERRA-2 has the lowest RMSE, and the poorest quality is observed for JRA-55.

In the ablation areas (Fig. 2b and d, Table 3b), MB shows an opposite seasonal cycle, with warm biases in summer and cold biases in winter for all datasets except for CFSR. Despite negative MB for any month in

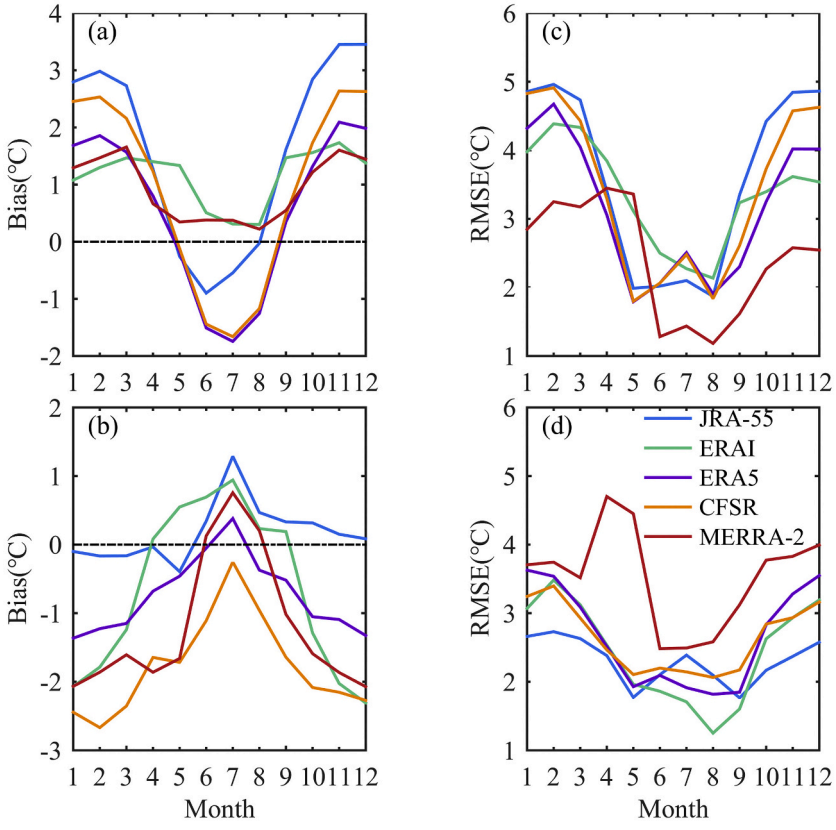

Fig. 2. Mean bias (MB) (a, b) and root-mean-square error (RMSE) (c, d) of monthly air temperature in all reanalysis datasets with respective to the corresponding observations from the stations above 1500 m elevation (a, c) and below 1500 m elevation (b, d).

Table 3
Overall skill statistics of the five near-surface air temperature reanalysis.

Name	Ablation area								Accumulation area							
	Spring		Summer		Autumn		Winter		Spring		Summer		Autumn		Winter	
	MB/ °C	RMSE/ °C	MB/ °C	RMSE/ °C	MB/ °C	RMSE/ °C	MB/ °C	RMSE/ °C	MB/ °C	RMSE/ °C	MB/ °C	RMSE/ °C	MB/ °C	RMSE/ °C	MB/ °C	RMSE/ °C
JRA-55	1.25	3.38	−0.49	2.00	2.64	4.21	3.08	4.88	−0.20	2.26	0.70	2.20	0.27	2.10	−0.06	2.66
ERAI	1.40	3.76	0.37	2.30	1.59	3.42	1.25	3.97	−0.20	2.54	0.62	1.61	−1.04	2.39	−2.05	3.20
ERA5	0.73	2.97	−1.50	2.16	1.25	3.19	1.84	4.33	−0.76	2.51	−0.01	1.94	−0.89	2.65	−1.31	3.59
CFSR	1.09	3.18	−1.42	2.13	1.61	3.64	2.54	4.80	−1.91	2.50	−0.77	2.14	−1.96	2.65	−2.46	3.26
MERRA2	0.89	3.33	0.32	1.30	1.12	2.16	1.40	2.87	−1.71	4.22	0.36	2.52	−1.49	3.58	−2.00	3.79

CFSR, the absolute value of MB is still smallest in summer. Seasonality of RMSE is similar to that in the accumulation areas, with the smallest values in summer and the highest values in winter. Among the reanalysis datasets, MERRA-2 shows the largest RMSE at all months, indicating poor performance for the entire year. The differences of RMSEs between ERAI and ERA5 are small, suggesting no significant improvement of ERA5, compared with ERAI.

Overall, the quality of all reanalysis products is seasonally dependent, more reliable in summer and less reliable in winter. MERRA-2 is considered the best performer for air temperature in the accumulation areas, whereas JRA-55 shows the best performance for the ablation areas.

3.1.2. *Relative humidity*

Under the condition of constant specific humidity, relative humidity is inversely proportional to temperature. And when relative humidity is constant, temperature is directly related to the specific humidity.

The intra-annual cycle of MB and RMSE of relative humidity from all reanalysis datasets is shown in Fig. 3 and Table 4. Similar seasonal cycles of MB of JRA55, ERAI and ERA5 are observed in the accumulation areas and ablation areas (Fig. 4a and c). However, unlike the other three datasets, CFSR and MERRA-2 exhibit no clear variations in MB. MB of JRA55, ERAI and ERA5 are negative for any month, indicating that all monthly relative humidity values are underestimated by these datasets. In contrary, MBs in CFSR are positive throughout 12 months for the ablation areas. Over the same region, MB values of MERRA-2 in each month are approximately zero, indicating a high performance of MERRA-2. Concerning the RMSE, similar intra-annual changes are found for all reanalysis datasets for both regions, peaking during winter months (Fig. 3b and d). This demonstrates that the poorest performance of all products occurs in winter. Compared with ERAI, ERA5 presents a slightly lower RMSE for the region in accumulation areas (Fig. 3c), but higher RMSE in the ablation areas (Fig. 3d). MERRA-2 performs nearly as well as CFSR for the accumulation area, whereas the quality of MERRA-2 is higher between March and September for the ablation areas.

Among the datasets, ERAI has the lowest performance in the accumulation area, and in ablation area, ERA5 performs worst. CFSR ranks first for the accumulation areas, while in the ablation areas, MERRA-2 shows the highest skill for representing relative humidity.

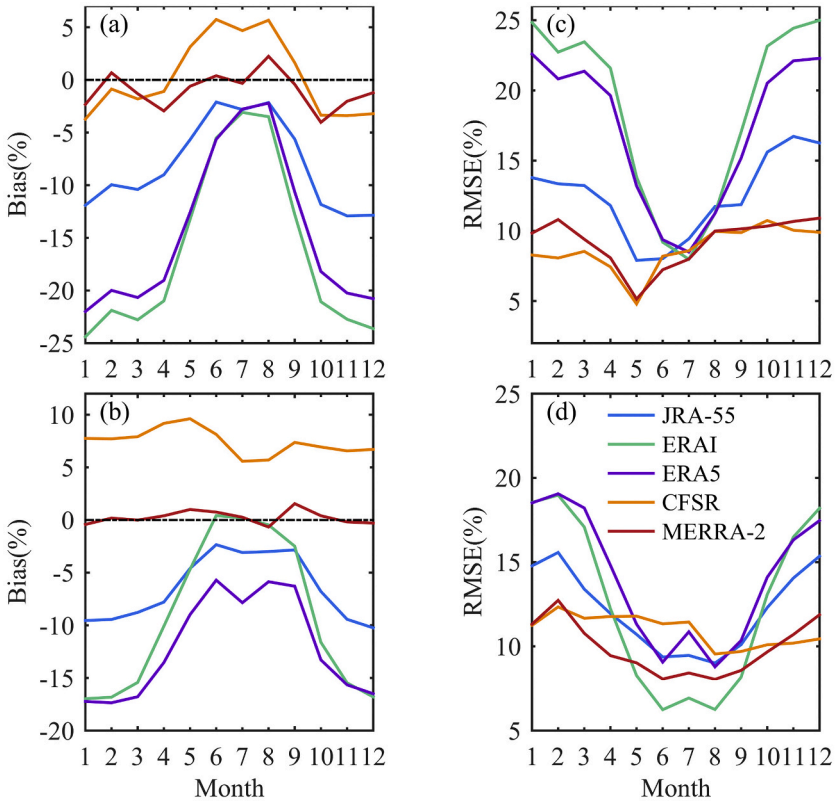

Fig. 3. As in Figure2, but for relative humidity (%).

Table 4
As in Table 3, but for relative humidity.

Name	Ablation area								Accumulation area							
	Spring		Summer		Autumn		Winter		Spring		Summer		Autumn		Winter	
	MB/°C	RMSE/°C	MB/°C	RMSE/°C	MB/°C	RMSE/°C	MB/°C	RMSE/°C	MB/°C	RMSE/°C	MB/°C	RMSE/°C	MB/°C	RMSE/°C	MB/°C	RMSE/°C
JRA-55	−8.37	10.97	−2.36	9.72	−10.12	14.73	−11.57	14.29	−4.91	10.68	−2.98	9.52	−8.82	13.90	−9.11	14.85
ERAI	−19.01	19.63	−4.03	9.47	−18.86	21.54	−23.30	24.35	−4.78	8.92	−0.92	7.12	−14.63	15.92	−16.12	18.35
ERA5	−17.44	18.07	−3.54	9.70	−16.36	19.27	−20.92	22.07	−9.41	11.73	−6.67	10.00	−15.15	15.96	−17.07	18.78
CFSR	0.07	6.92	5.36	8.91	−1.70	10.22	−2.60	8.63	8.98	11.63	6.21	10.23	6.73	10.24	7.81	12.12
MERRA2	−1.62	7.54	0.77	8.40	−2.16	10.38	−0.96	10.34	0.72	8.84	0.38	8.35	−0.03	10.75	0.09	12.08

3.1.3. Wind speed

The MB and RMSE of wind speed from the five reanalysis datasets in the accumulation areas and ablation areas, respectively, are presented in Fig. 4 and Table 5. At both regions, MERRA-2 has positive MB, whereas negative MB values are observed in CFSR and ERA5 at any month. ERAI indicates negative MB at all months but February. All monthly MB values of JRA-55 are negative for ablation areas (Fig. 4a), but for accumulation areas (Fig. 4b), a positive MB is present during October–February.

At ablation regions, all reanalysis products, aside from MERRA-2 (Fig. 4c), have larger deviation than the corresponding months at accumulation areas (Fig. 4a). In addition, it is obvious that monthly RMSE values over ablation areas (Fig. 4d) of all reanalysis datasets but MERRA-2, are larger than the corresponding months over accumulation areas (Fig. 4c). This suggests that the skills of all reanalyses (except MERRA-2) for representing wind speeds over accumulation areas outperform for ablation areas. Distinct seasonality is found for the RMSE of all datasets excluding JRA-55 over both regions, with higher values during winter months, and relatively smaller values during summer months. In particular, over accumulation zone elevations, seasonal fluctuation of RMSE of MERRA-2 is largest among all datasets. RSME values of ERA5 are smaller than ERAI for all months excluding March. By comparison, the quality of ERA5 is best for the wind speeds over the accumulation areas, with the averaged RMSE of 1.40 m s^{-1}. Nevertheless, JRA-55 has an average RMSE of 1.80 m s^{-1}, and outperforms the other datasets for ablation areas elevations.

3.2. Inter-comparison between the reanalysis datasets

3.2.1. Air temperature

Fig. 5a presents the time series of anomalies of area-weighted annual 2 m air temperature of five reanalysis products from 1980 to 2018, relative to 1980–2018 mean, averaged over the GrIS (60–84°N, 295–340°E). Inter-annual variability in mean annual 2 m air temperature of each reanalysis product shows high correlations (r), with the correlation coefficients of >0.99 ($p < 0.01$). The GrIS air temperature of each reanalysis dataset is lower than the average from 1980 to mid-1990, followed by a sharp increase to the 2000s and then a slight decreases until 2018. From 1980 to 2018, the significant warming trends are comparable for all reanalysis datasets (Table 6).

The statistics of the average air temperature trends for the GrIS for all reanalysis products for the 1980–2018 periods are shown in Fig. 5b. The mean and median trends in JRA-55 are the largest of all the datasets and ERAI ranks second. ERA5 and CFSR show almost identical median and average trend values, which are lower than those for ERAI. Evident differences in the distribution of trends are also found between the reanalysis products. CFSR experiences larger trend range than the other reanalyses. The largest number of positive extreme trend values occurs in CFSR, and MERRA-2 indicates more negative extreme trend values than the other reanalysis products.

3.2.2. Relative humidity

Interannual variability in relative humidity of ERAI agrees well with ERA5, with the r value of 0.98 ($p < 0.01$) (Fig. 6a). Some common year-to-year changes also occur across the other datasets. However, evident differences are observed. JRA-55 departs distinctly from the other reanalyses during the early 1990s, and from 2010 onwards. In particular, the sudden decrease in relative humidity after 2009 in JRA-55 appears to be spurious. Despite the same sign of trends for the 1980–2018 period, more negative trend values are seen for JRA-55 (Table 3). As shown in Fig. 7b, JRA-55 shows the largest trend range, and the largest number of positive extreme values occurs in CFSR. Although certain differences are present in the relative humidity from the ERAI, ERA5 and CFSR, especially in the outlier values, their trend distributions are similar.

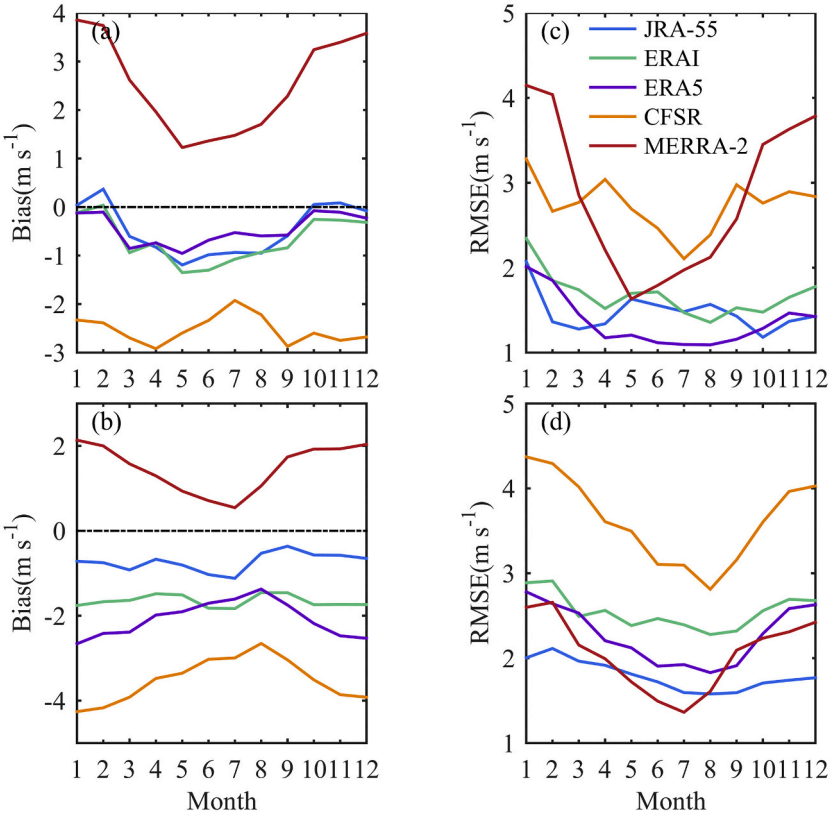

Fig. 4. As in Figure2, but for wind speed (m s-1).

3.2.3. Wind speed

Time series of annual mean wind speed anomalies in the five reanalysis products during 1980–2018 over GrIS are shown in Fig. 7a. The high and significant correlations between these time series ($r > 0.99$, $p < 0.01$) reveal the robust agreement of inter-annual variability in the wind speed from the five reanalyses. Despite the consistency, there are clear discrepancies for their trends. The long-term (1980–2014) trends are small and not significant for JRA-55 and ERAI, but significantly positive for ERA5, CFSR and MERRA-2. It is notable that CFSR exhibits a sharp jump of area averaged wind speed over the GrIS from 2010 to 2011, probably due to the inhomogeneities of two versions of CFSR. Thus, its trend for the 1980–2010 period could be spurious. It also explains the larger amount of extreme values in CFSR trend distribution (Fig. 8b). Between the reanalysis datasets, their trend distributions are different. For MERRA-2, about 75% of grids experience upward trends, but downward trends are observed for >50% grids of JRA-55. ERAI shows the smallest trend distribution range, and in contrast, the largest trend distribution range is in CFSR.

4. Discussion

We use AWS measurements from 1996 to 2018 to evaluate the skills of the five reanalysis products for capturing air temperature, relative humidity and wind speed over the GrIS.

The quality of the reanalysis datasets is seasonally dependent, with better performance for the three meteorological variables during summer than during winter. In winter, katabatic forcing is the dominant momentum of the atmospheric boundary layer over the GrIS, which usually leads to a temperature deficit, and direction-constant and strong near-surface winds, and greatly affects relative humidity. In summer, the atmospheric boundary layer on the ice sheet is largely forced by large-scale circulation (Ettema et al., 2010; Van Angelen et al., 2011). In addition, the smaller summer time bias will be influenced by the melting ice surface. Global reanalyses generally represent large-scale atmospheric circulation well, but not katabatic forcings (Bracegirdle and Marshall, 2012). An additional possible explanation for air temperature biases is a missing representation of snow in the reanalyses products. Batrak and Müller (2019) reported temperature biases of global reanalyses in the Arctic as a function of thickness of the snow layer. The thicker snow-depths co-exist with lower temperatures and larger biases in the reanalyses. At the ice sheet scale, the thinner snow in summer than in winter is well known. Furthermore, too weak surface temperature inversions in winter simulated by the global atmospheric reanalysis is also a possible reason (Tjernström and Graversen, 2009; Graham et al., 2019).

Previous studies reported that seasonal variability in environmental lapse rates of temperature occurs in the mountainous regions, such as in the Alpine area, with higher values in summer, and lower values in winter (Rolland, 2003). Thus, it should apply the monthly environmental lapse rate for elevation correction when calculating MB and RMSE of monthly air temperature from reanalysis datasets. In this study, we use only one value (6.5 °C/km) for all months, which results in the difference of the calculated monthly MB and RMSE with those estimated based on monthly environmental lapse rates. However, the monthly lapse rates cannot be estimated by the insufficient AWS station observations over the GrIS. Furthermore, the location factors resulting from the scattered distribution of AWSs cannot easily be excluded when calculating monthly vertical lapse rates. Although only one environment lapse rate is considered, the RMSE after elevation corrections decreases compared with those without the elevation correction (Fig. S1).

The AWS wind speed measurements are typically at 3 m above the surface. To estimate the 10 m wind speed from the reanalysis datasets, it is necessary to extrapolate the observed wind speeds to 10-m height. While there is no large difference in the RMSE between applying extrapolation and not applying extrapolation at the ablation zone, the RMSE of all reanalyses obviously decreases for the accumulation area

Table 5
As in Table 3, but for wind speed.

Ablation area								Accumulation area							
name	Spring		Summer		Autumn		Winter		Spring		Summer		Autumn		Winter	
	MB/°C	RMSE/°C	MB/°C	RMSE/°C	MB/°C	RMSE/°C	MB/°C	RMSE/°C	MB/°C	RMSE/°C	MB/°C	RMSE/°C	MB/°C	RMSE/°C	MB/°C	RMSE/°C
JRA-55	−0.85	1.48	−0.97	1.54	−0.16	1.32	0.13	1.78	−0.81	1.84	−0.67	1.59	−0.60	1.74	−0.80	2.06
ERAI	−0.98	1.68	−1.12	1.52	−0.45	1.55	−0.11	2.07	−1.59	2.54	−1.59	2.34	−1.74	2.64	−1.63	2.80
ERA5	−0.82	1.34	−0.62	1.12	−0.26	1.30	−0.13	1.86	−1.85	2.12	−1.58	1.89	−2.40	2.50	−2.38	2.61
CFSR	−2.71	2.85	−2.18	2.33	−2.73	2.87	−2.43	3.02	−3.30	3.43	−2.90	3.02	−3.77	3.87	−4.03	4.21
MERRA2	1.97	2.30	1.49	1.95	2.97	3.22	3.75	4.07	1.02	1.80	1.11	1.69	1.96	2.32	1.82	2.51

after using extrapolation (Fig. S2).

The GrIS is experiencing mass loss since 1998 (Mouginot et al., 2019), and cause the rise of ELA. However, the changes in ELA cannot significantly affect the MB and RMSE calculations in the respective region because only one station is near ELA.

No single reanalysis dataset is optimal for the representation of all three variables (air temperature, relative humidity and wind speed) over the GrIS. MERRA-2 outperforms the other four reanalysis dataset for air temperature in the accumulation area, but the quality of JRA-55 ranks first in the ablation areas. In terms of relative humidity, CFSR performs best for the accumulation areas, but for the ablation areas, MERRA-2 does the best job, while ERA5 and JRA-55 show the best performance for capturing wind speeds in the accumulation area and in the ablation area, respectively. This indicates that the simulation skill varies for each variable, location, and weather pattern in all reanalyses. This may result from the distinct boundary layer routines and varying observation systems assimilated in the different models that are used to produce the corresponding reanalysis datasets. For instance, in the ice sheet margins, the quality of the reanalyses for local climate is to a great extent dependent on their skills of capturing sea-ice distribution in the surface boundary conditions (Renfrew et al., 2020). The different resolutions of the reanalyses may also play a role in the uncertainties of the variables, but it could not be discriminated from the other factors, such as the assimilation scheme and data, resulting in errors of different reanalyses. As a result, despite the much higher spatial and temporal resolution of ERA5, this reanalysis does not perform significantly better, and performs even worse for some surface meteorology parameters, relative to other reanalyses.

The time series of annual air temperature, relative humidity and wind speed averaged over the GrIS show significant and high correlations across the five reanalysis datasets, suggesting robust agreements of their respective inter-annual variability. This can be explained by their similar performance for the large scale atmospheric circulation and partly same data assimilated in the products. However, a sharp decrease in relative humidity is observed in JRA-55, and a sudden increase is observed in wind speed in CFSR from 2010 to 2011. For CFSR, the bridge year 2010, i.e., the end of the CFSRv1 and the start of the CFSv2 extension, has been found to characterize inhomogeneities in other meteorological parameters, such as stratospheric water vapor (Davis et al., 2017), high-cloud fraction (Wright et al., 2020). For JRA-55, sharp shifts in snow accumulation have been reported by Wang et al. (*2016*). Fig. 8 shows spatial distribution of the differences in wind speeds from CFSR, and relative humidity from JRA-55, between the 2002–2009 mean and 2011–2018 mean. Large increases are observed over the coastal region of the GrIS for the wind speed for the first 8 years of CFSRv2 (2011–2018), relative to the last 8 years of CFSRv1 (2002–2009), which leads to the sudden jump in the ice sheet averaged wind speed time series. In JRA-55, the western, northeastern, and southern GrIS coastal regions exhibit a decrease of >5% in the 2002–2009 relative humidity average compared to the 2011–2018 mean. A slighter decrease is also found in almost all the inland GrIS.

5. Conclusion

In this study, we assess the skills of five reanalysis datasets (i.e., JRA-55, MERRA-2, CFSR, ERAI and ERA5) for representing air temperature, relative humidity and wind speed over the GrIS based on in situ measurements from 36 AWS stations. These stations are divided into two groups, one above the approximate equilibrium line altitude (1500 m elevation), i.e., the accumulation zone, and another below 1500 m elevation, i.e., the ablation zone.

With respect to the observed air temperature in winter, all reanalysis datasets show warm biases for the accumulation zone, but cold biases for the ablation zone. By comparison, MERRA-2 is the best performer at the accumulation area and the quality of JRA-55 ranks first at ablation area. Relative to the ERAI, there is no significant improvement of ERA5. At

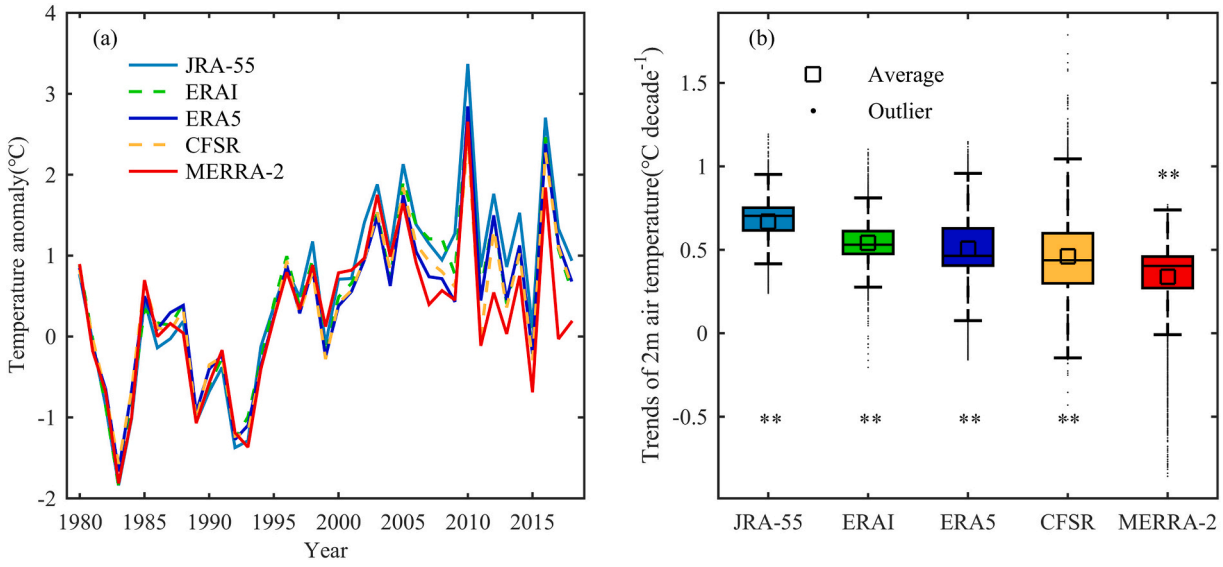

Fig. 5. (a) Time series of anomalies of annual 2 m air temperature from 1980 to 2018 from five reanalyses, relative to respective 1980–2018 mean, spatially averaged over the GrIS (60–84°N, 295–340°E); (b) Boxplot showing the distributions of temperature trends in each grid cell of five reanalysis datasets. The box spans the upper (3/4) and lower (1/4) quartiles. Black square and line inside the box stand for the average and median trends, respectively. The whiskers denote the 95% bounds, and the points beyond the whiskers are the outliers. The "**" denotes that trends are significant at the 95% confidence level.

Table 6
Trends in annual air temperature, relative humidity and wind speeds from the reanalysis datasets during 1980–2018, averaged over the GrIS (60–84°N , 295–340°E). The bold fonts show that trends are significant at the 95% confidence level.

Datasets	Air temperature (°C)	Relative humidity (%)	Wind speeds (m s^{-1})
JRA-55	**0.69 ± 0.12**	**−1.13 ± 012**	−0.01 ± 0.02
ERAI	**0.54 ± 0.11**	**−0.32 ± 0.08**	0.01 ± 0.01
ERA5	**0.49 ± 0.11**	**−0.21 ± 0.08**	**0.02 ± 0.01**
CFSR	**0.46 ± 0.11**	**−0.21 ± 0.05**	**0.08 ± 0.01**
MERRA-2	**0.36 ± 0.12**	**−0.29 ± 0.07**	**0.04 ± 0.02**

both accumulation and ablation zones, JRA-55 and two ECMWF reanalyses underestimate the relative humidity at all months. When compared with the other reanalysis datasets, MERRA-2 appears to capture the best seasonal cycle of the observed relative humidity. ERA5 performs better than ERAI at the accumulation zone, but poorer in the ablation zone. MERRA-2 overestimates averaged wind speed at any month, whereas underestimation is found for the other reanalysis products. While JRA-55 has the highest skill for representing the monthly wind speed over the ablation zone, ERA5 does the best job for the accumulation zone. In a word, no reanalysis stands out as the optimal performance for all three variables and glaciological regimes.

Time series of anomalies of annual air temperature from the five reanalyses averaged over the GrIS agree well with each other. The roust agreements between the reanalysis datasets also happen for the time series of annual relative humidity and wind speed. However, JRA-55 exhibits a sharp shift of relative humidity from 2010 to 2011. During the same period, evident discontinuities occur in the annual mean wind speed from CFSR. Thus, cautions should be taken in application of the two reanalysis datasets for the trend investigations, especially when spanning the 2010 year. Future work is needed to explain this in detail.

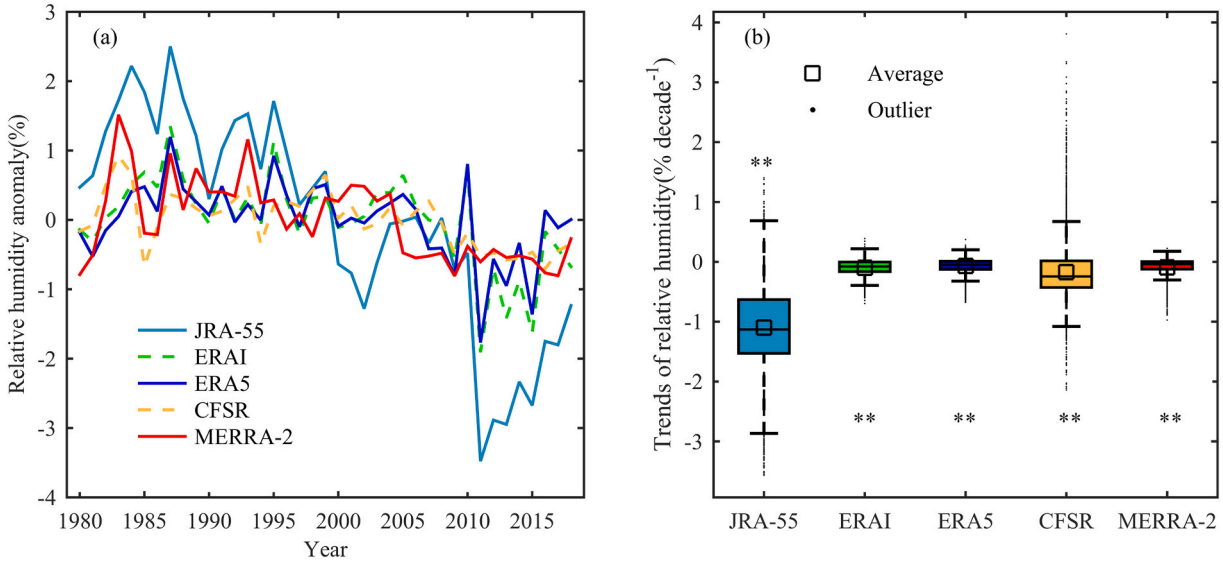

Fig. 6. As in Figure5, but for relative humidity (%).

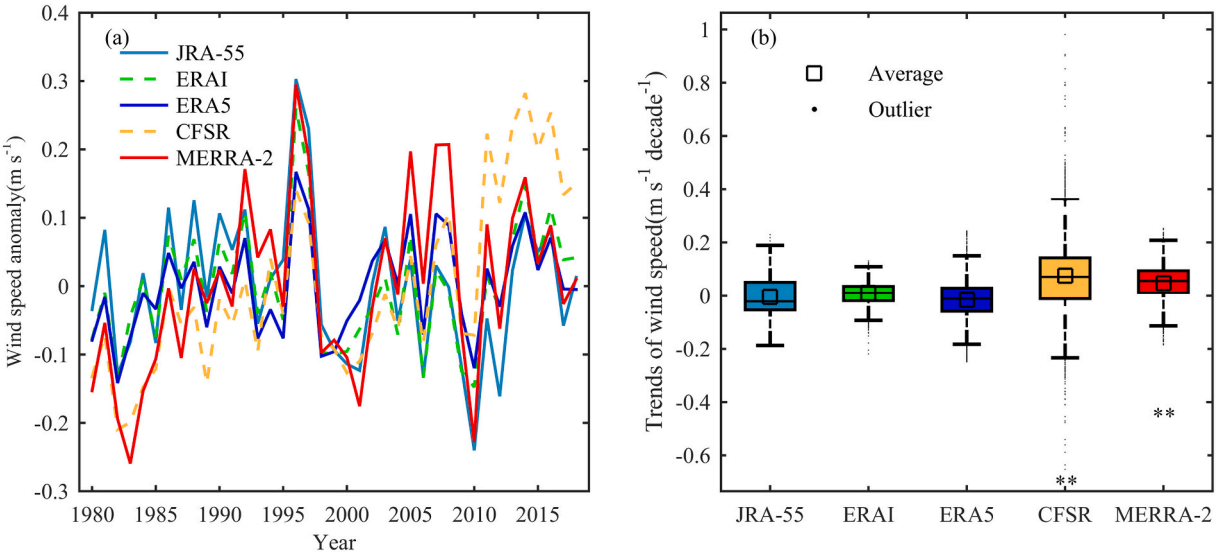

Fig. 7. As in Fig. 5, but for wind speed (m s^{-1}).

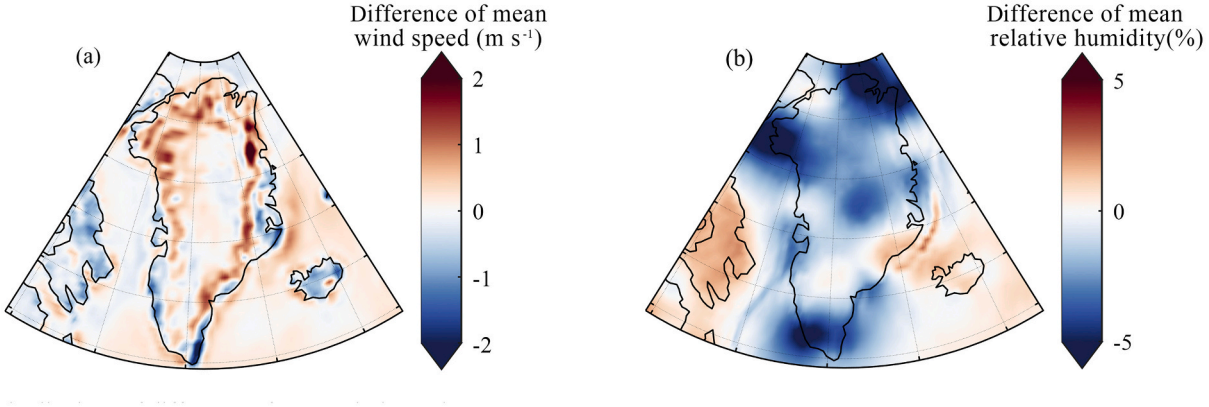

Fig. 8. Distributions of difference of meteorological elements between different periods (a) wind speed for CFSR and (b) relative humidity for JRA-55.

Author statement

Zhang Wuying: Conceptualization, Software, Writing-original draft.
Wang Yetang: Data curation, Writing-reviewing and Editing.
Paul C. J. P. Smeets: Data curation, Writing-review & editing.
Carleen H. Reijmer: Data curation, Writing-review & editing.
Baojuan Huai: Software, Validation.
Wang Junyao: Software, Validation.
Weijun Sun: Writing-reviewing and Editing.

Declaration of Competing Interest

The authors declare that they have no known competing financial interests or personal relationships that could have appeared to influence the work reported in this paper.

Acknowledgements

Funding this work was the National Natural Science Foundation of China (41971081), the Project for Outstanding Youth Innovation Team in the Universities of Shandong Province (2019KJH011), the Strategic Priority Research Program of the Chinese Academy of Sciences (XAD19070103), and the Outstanding Youth Fund of Shandong Provincial Universities (ZR2016JL030).

Appendix A. Supplementary data

Supplementary data to this article can be found online at https://doi.org/10.1016/j.atmosres.2021.105676.

References

Batrak, Y., Müller, M., 2019. On the warm bias in atmospheric reanalyses induced by the missing snow over Arctic Sea-ice. Nat. Commun. 10 (1), 1–8. https://doi.org/10.1038/s41467-019-11975-3.

Berrisford, P., Kållberg, P., Kobayashi, S., Dee, D., Uppala, S., Simmons, A.J., Poli, P., Sato, H., 2011. Atmospheric conservation properties in ERA-Interim. Quart. J. Roy. Meteor. Soc. 137 (659), 1381–1399. https://doi.org/10.1002/qj.864.

Bracegirdle, T.J., Marshall, G.J., 2012. The Reliability of Antarctic Tropospheric pressure and Temperature in the latest Global Reanalyses. J. Clim. 25 (20), 7138–7146. https://doi.org/10.1175/JCLI-D-11-00685.1.

Chylek, P., Box, J.E., Lesins, G., 2004. Global Warming and the Greenland Ice Sheet. Clim. Chang. 63 (1–2), 201–221. https://doi.org/10.1023/B:CLIM.0000018509.74228.03.

Davis, S.M., Hegglin, M.I., Fujiwara, M., Dragani, R., Harada, Y., Kobayashi, C., Long, C., Manney, G.L., Nash, E.R., Potter, G.L., Tegtmeier, S., Wang, T., Wargan, K., Wright, J.S., 2017. Assessment of upper tropospheric and stratospheric water vapor and ozone in reanalyses as part of S-RIP. Atmos. Chem. Phys. 17 (20), 12743–12778. https://doi.org/10.5194/acp-17-12743-2017.

Dee, D.P., Uppala, S.M., Simmons, A.J., Berrisford, P., Poli, P., Kobayashi, S., Andraec, U., Balmaseda, M.A., Balsamo, G., Bauer, P., Bechtold, P., Beljaars, A.C.M., van de Berg, L., Bidlot, J., Bormann, N., Delsol, C., Dragani, R., Fuentes, M., Geer, A. J., Haimberger, L., Healy, S.B., Hersbach, H., Hólma, E.V., Isaksen, L., Kållbergc, P., Köhlera, M., Matricardi, M., McNally, A.P., Monge-Sanz, B.M., Morcrette, J.-J., Park, B.-K., Peubey, C., de Rosnay, P., Tavolato, C., Thépaut, J.-N., Vitart, F., 2011.

The ERA-Interim reanalysis: Configuration and performance of the data assimilation system. Q. J. R. Meteorol. Soc. 137 (656), 553–597. https://doi.org/10.1002/qj.828.
Delhasse, A., Kittel, C., Amory, C., Hofer, S., Fettweis, X., 2019. Brief communication: interest of a regional climate model against ERA5 to simulate the near-surface climate of the Greenland ice. Cryosphere Dis. 1–12. https://doi.org/10.5194/tc-2019-96.
Dong, X., Wang, Y., Hou, S., Ding, M., Zhang, Y., 2020. Robustness of the recent global atmospheric reanalyses for antarctic near-surface wind speed climatology. J. Clim. 33 (10) https://doi.org/10.1175/JCLI-D-19-0648.1.
Ebita, A., Kobayashi, S., Ota, Y., Moriya, Masami, Kumabe, R., Onogi, K., Harada, Y., Yasui, S., Miyaoka, K., Takahashi, K., Kamahori, H., Kobayashi, C., Endo, H., Soma, M., Oikawa, Y., Ishimizu, T., 2011. The Japanese 55-year reanalysis "JRA-55": an Interim report. Sola. 7, 149–152. https://doi.org/10.2151/sola.2011-038.
Ettema, J., van den Broeke, M.R., van Meijgaard, E., van de Berg, W.J., Box, J.E., Steffen, K., 2010. Climate of the Greenland ice sheet using a high-resolution climate model – part 1: Evaluation. Cryosphere 4 (4). https://doi.org/10.5194/tc-4-511-2010.
Eyre, J.E.J.R., Zeng, X., 2017. Evaluation of Greenland near surface air temperature datasets. Cryosphere Dis. 11 (4), 1–28. https://doi.org/10.5194/tc-11-1591-2017.
Gelaro, R., McCarty, W., Suárez, M.J., Todling, R., Molod, A., Takacs, L., Randles, C.A., Darmenov, A., Bosilovich, M.G., Reichle, R., Wargan, K., Coy, L., Cullather, R., Draper, C., Akella, S., Buchard, V., Conaty, A., Da Silva, A.M., Gu, W., Kim, G., Koster, R., Lucchesi, R., Merkova, D., Nielsen, J.E., Partyka, G., Pawson, S., Putman, W., Rienecker, M., Schubert, S.D., Sienkiewicz, M., Zhao, Bin, 2017. The Modern-Era Retrospective analysis for research and applications, Version 2 (MERRA-2). J. Clim. 30, 5419–5454. https://doi.org/10.1175/JCLI-D-16-0758.1.
Gillet-Chaulet, F., Gagliardini, O., Seddik, H., Nodet, M., Durand, G., Ritz, C., Zwinger, T., Greve, R., Vaughan, D.G., 2012. Greenland ice sheet contribution to sea-level rise from a new-generation ice-sheet model. Cryosphere 6, 1561–1576. https://doi.org/10.5194/tc-6-1561-2012.
Graham, R.M., Cohen, L., Ritzhaupt, N., Segger, B., Graversen, R.G., Rinke, A., Walden, V.P., Granskog, M.A., Hudson, S.R., 2019. Evaluation of six atmospheric reanalyses over arctic Sea Ice from Winter to early Summer. J. Clim. 32, 4121–4143. https://doi.org/10.1175/JCLI-D-18-0643.1.
Hanna, E., Valdes, P., Mcconnell, J., 2010. Patterns and Variations of Snow Accumulation over Greenland, 1979-98, from ECMWF analyses, and their Verification. J. Clim. 14 (17), 3521–3535. https://doi.org/10.1175/1520-0442(2001)0142.0.CO;2.
Hanna, E., Fettweis, X., Hall, R.J., 2018. Brief communication: recent changes in summer Greenland blocking captured by none of the CMIP5 models. Cryosphere, 2018 12 (10), 3287–3292. https://doi.org/10.5194/tc-12-3287-2018-supplement.
Hearty, T.J., Lee, J.N., Wu, D.L., Cullather, R., Blaisdell, J.M., Susskind, J., Nowicki, S.M. J., 2018. Intercomparison of surface temperatures from AIRS, MERRA, and MERRA-2 with NOAA and GC-Net weather stations at summit, Greenland. J. Appl. Meteorol. Climatol. 57 (5), 1231–1245. https://doi.org/10.1175/JAMC-D-17-0216.1.
Hennermann, K., Berrisford, P., 2017. ERA5 data documentation (Copernicus knowledge base).
Hersbach, H., Dee, D., 2016. ERA5 reanalysis is in production. ECMWF. Newslett. 147, 7.
Hsu, S.A., Meindl, E.A., Gilhousen, D.B., 1994. Determining the power-law wind-profile exponent under near-neutral stability conditions at sea. J. Appl. Meteorol. 33 (6), 757–765. https://doi.org/10.1175/1520-0450(1994)033<0757:DTPLWP>2.0.CO;2.
IPCC, 2019: Summary for policymakers, IPCC Special Report on the Ocean and Cryosphere in a Changing Climate [Pörtner, H.-O., Roberts, D. C., Masson-Delmotte, V, Zhai, P, Tignor, M., Poloczanska, E., Mintenbeck, K., Nicolai, M., Okem, A., Petzold, J., Rama, B., Weyer, N]. In press.
Johnson, J., 1995. Turbulent heat flux measurements over the Greenland, Norwegian and Barents seas (M. S. Thesis).
Katul, G., Parlange, M., 1994. On the active role of temperature in surface-layer turbulence. J. Atmos. Sci. 51 (15), 2181–2195. https://doi.org/10.1175/1520-0469(1994)051<2181:otarot>2.0.co;2.
Kobayashi, S., Ota, Y., Harada, Y., Ebita, A., Moriya, M., Onoda, H., Onogi, K., Kamahori, H., Kobayashi, C., Endo, H., Miyaoka, K., Takahashi, K., 2015. The JRA-55 Reanalysis: General specification and basic characteristics. J. Meteorol. Soc. Jpn. 93, 5–48. https://doi.org/10.2151/jmsj.2015-001.
Lazzara, M.A., Keller, L.M., Thom, J.E., 2012. Antarctic automatic weather station program: 30 years of polar observation. Bull. Am. Meteorol. Soc. 93 (10), 1519–1537. https://doi.org/10.1175/BAMS-D-11-00015.1.
Li, G., Ren, B., Yang, C., Zheng, J., 2011. Revisiting the trend of the tropical and subtropical Pacific surface latent heat flux during 1977–2006. J. Geophys. Res. 116, D10115. https://doi.org/10.1029/2010JD015444, 2011.
Marray, W., 1967. On the computation of saturation vapor pressure. J. Appl. Meterol. 6 (1), 203–204.
Mouginot, J., Rignot, E., Bjørk, A.A., Van den Broeke, M.R., Millan, R., Morlighem, M., Noël, B., Scheuchl, B., Wood, M., 2019. Forty-six years of Greenland ice sheet mass balance from 1972 to 2018. Proc. Natl. Acad. Sci. 116 (19) https://doi.org/10.1073/pnas.1904242116.
Munneke, P.K., Smeets, P.C.J.P., Oerlemans, J., van de Wal, R.S.W., van den Broeke, M. R., 2018. The K-transect in West Greenland: Automatic weather station data (1993-2016). Arct. Antarct. Alp. Res. 50 (1), e1420952 https://doi.org/10.1080/15230430.2017.1420952.
Overland, J.E., Wang, M., 2016. Recent Extreme Arctic Temperatures are due to a Split Polar Vortex. J. Clim. 29 (15), 5609–5616. https://doi.org/10.1175/JCLI-D-16-0320.1.
Paulson, C.A., 1970. The mathematical representation of wind speed and temperature profiles in the unstable atmospheric surface layer. J. Appl. Meteorol. 9, 857–861. https://doi.org/10.1175/1520-0450(1970)009<0857:TMROWS>2.0.CO;2.
Ren, D., Fu, R., Leslie, L.M., Karoly, D.J., Chen, J., Wilson, C., 2011. A multirheology ice model: formulation and application to the Greenland ice sheet. J. Geophys. Res. 116, D05112 https://doi.org/10.1029/2010JD014855.
Renfrew, I.A., Barrell, C., Elvidge, A.D., Brooke, J.K., Duscha, C., King, J.C., Kristiansen, J., Cope, L.T., Moore, G.W.K., Pickart, R.S., Reuder, J., Sandu, I., Sergeev, D., Terpstra, A., Våge, K., Weiss, A., 2020. An evaluation of surface meteorology and fluxes over the Iceland and Greenland Seas in ERA5 reanalysis: the impact of sea ice distribution. Q. J. R. Meteorol. Soc. 1-22 https://doi.org/10.1002/qj.3941.
Rolland, C., 2003. Spatial and seasonal variations of air temperature lapse rates in alpine regions. J. Clim. 16 (7), 1032–1046. https://doi.org/10.1175/1520-0442(2003)016<1032:SASVOA>2.0.CO;2.
Saha, S., Nadiga, S., Thiaw, C., Wang, J., Wang, W., Zhang, Q., van den Dool, H.M., Moorthi, H.-L.P., Behringer, D., PEÑA, M., Lord, S., White, G., Ebisuzake, W., Peng, P., Xie, P., 2006. The NCEP climate forecast system. J. Clim. 19, 3483–3517. https://doi.org/10.1175/JCLI3812.1.
Saha, S., Moorthi, S., Pan, H.-L., Wu, X., Wang, J., Nadiga, S., Tripp, P., Kistler, R., Woollen, J., Behringer, D., Liu, H., Stokes, D., Grumbine, R., Gayno, G., Wang, J., Hou, Y., Chuang, H., Juang, H.H., Sela, J., Iredell, M., Treadon, R., Kleist, D., van Delst, P., Keyoser, D., Derber, J., Ek, M., Meng, J., Wei, H., Yang, R., Lord, S., vab de Dool, H., Kumar, A., Wang, W., Long, C., Chelliah, M., Xue, Y., Huang, B., Schemm, J., Ebisuzaki, W., Lin, R., Xie, P., Chen, M., Zhou, S., Higgins, W., Zou, C., Liu, Q., Chen, Y., Han, Y., Cucurull, L., Reynolds, R.W., Rutledge, G., Goldberg, M., 2010. The NCEP climate forecast system reanalysis. Bull. Am. Meteorol. Soc. 91, 1015–1057. https://doi.org/10.1175/2010BAMS3001.1.
Saha, S., Moorthi, S., Wu, X., Wang, J., Nadiga, S., Tripp, P., Behringer, D., Hou, Y., Chuang, H., Iredell, M., Ek, M., Meng, J., Yang, R., Mendez, M.P., van de Dool, H., Zhang, Q., Wang, W., Chen, M., Becker, E., 2014. The NCEP climate forecast system version 2. J. Clim. 27 (6), 2185–2208. https://doi.org/10.1175/JCLI-D-12-00823.1.
Sanz Rodrigo, J., 2011. On Antarctic Wind Engineering. Ph.D. Thesis. Université Libre de Bruxelles, pp. 1–218.
Steffen, K., Box, J., 2001. Surface climatology of the Greenland Ice Sheet: Greenland climate Network 1995-1999[J]. J. Geophys. Res. 106 (D24), 33951–33964. https://doi.org/10.1029/2001JD900161.
Takahashi, T., Ohtsu, T., Yassin, M., Kato, S., Murakami, S., 2002. Turbulence characteristics of wind over a hill with a rough surface. J. Wind Eng. Ind. Aerodyn. 90 (12–15), 1697–1706. https://doi.org/10.1016/S0167-6105(02)00280-5.
Tjernström, M., Graversen, R.G., 2009. The vertical structure of the lower Arctic troposphere analysed from observations and the ERA-40 reanalysis. Q. J. R. Meteorol. Soc. 135 (639) https://doi.org/10.1002/qj.380.
Touma, J.S., 1977. Dependence of the wind profile power law on stability for various locations. J. Air Pollut. Control Assoc 27, 863–866. https://doi.org/10.1080/00022470.1977.10470503.
Van Angelen, J.H., van den Broeke, M.R., van de Berg, W.J., 2011. Momentum budget of the atmospheric boundary layer over the Greenland ice sheet and its surrounding seas. J. Geophys. Res. Atmos. 116, D10. https://doi.org/10.1029/2010JD015485.
Van As, D., Fausto, R.S., Ahlstrøm, A.P., Andersen, S.B., Andersen, M.L., Citterio, M., Edelvang, K., Gravesen, P., Machguth, H., Nick, F.M., Nislsen, S., Weidick, A., 2011. Programme for monitoring of the Greenland ice sheet (promice): first temperature and ablation records. Geol. Surv. Den. 23, 73–76. https://doi.org/10.5167/uzh-131209.
Van de Wal, R.S.W., Oerlemans, J., 1997. Modelling the short-term response of the Greenland ice-sheet to global warming. Clim. Dyn. 13 (10), 733–744. https://doi.org/10.1007/s003820050194.
Van de Wal, R.S.W., Greuell, W., van den Broeke, M.R., Reijmer, C.H., Oerlemans, J., 2005. Surface mass-balance observations and automatic weather station data along a transect near Kangerlussuaq, West Greenland. Ann. Glaciol. 42, 311–316. https://doi.org/10.3189/172756405781812529.
van den Broeke, M., Smeets, P., van de Wal, W., 2011. The seasonal cycle and interannual variability of surface energy balance and melt in the ablation zone of the West Greenland ice sheet. Cryosphere 5, 377–390. https://doi.org/10.5194/tc-5-377-2011.
Wang, Y., Ding, M., van Wessem, J.M., Schlosser, E., Altnau, S., van den Broeke, M.R., Lenaerts, J.T.M., Thomas, E.R., Isaksson, E., Wang, J., Sun, W., 2016. A comparison of antarctic ice sheet surface mass balance from atmospheric climate models and in situ observations. J. Clim. 29, 5317–5337. https://doi.org/10.1175/JCLI-D-15-0642.1.
Wright, J.S., Sun, X., Konopka, P., Krüger, K., Legras, B., Molod, A.M., Tegtmeier, S., Zhang, G.J., Zhao, X., 2020. Differences in tropical high clouds among reanalyses: origins and radiative impacts. Atmos. Chem. Phys. 20 (14), 8989–9030. https://doi.org/10.5194/acp-20-8989-2020.